SEDIMENTOLOGY the journal of the International Association of Sedimentologists

Sedimentology (2010) **57,** 252–272 doi: 10.1111/j.1365-3091.2009.01110.x

On the relationship between flow and suspended sediment transport over the crest of a sand dune, Río Paraná, Argentina

DAN H. SHUGAR*[1], RAY KOSTASCHUK*, JAMES L. BEST†, DANIEL R. PARSONS‡, STUART N. LANE§, OSCAR ORFEO¶ and RICHARD J. HARDY§

**Department of Geography, University of Guelph, Guelph, ON, N1G 2W1, Canada (E-mail: dshugar@sfu.ca)*

†Departments of Geology and Geography and Ven Te Chow Hydrosystems Laboratory, University of Illinois, 1301 W. Green St., Urbana, IL 61801, USA

‡Earth and Biosphere Institute, School of Earth and Environment, University of Leeds, Leeds, West Yorkshire LS2 9JT, UK

§Department of Geography, Durham University, Durham DH1 3LE, UK

¶Centro de Ecología Aplicada del Litoral (CECOAL-CONICET), C.C. 291, 3400 Corrientes, Argentina

ABSTRACT

The links between large-scale turbulence and the suspension of sediment over alluvial bedforms have generated considerable interest in the last few decades, with past studies illustrating the origin of such turbulence and its influence on flow resistance, sediment transport and bedform morphology. In this study of turbulence and sediment suspension over large sand dunes in the Río Paraná, Argentina, time series of three-dimensional velocity, and at-a-point suspended sediment concentration and particle-size, were measured with an acoustic Doppler current profiler and laser *in situ* scattering transmissometer, respectively. These time series were decomposed using wavelet analysis to investigate the scales of covariation of flow velocity and suspended sediment. The analysis reveals an inverse relationship between streamwise and vertical velocities over the dune crest, where streamwise flow deceleration is linked to the vertical flux of fluid towards the water surface in the form of large turbulent fluid ejections. Regions of high suspended sediment concentration are found to correlate well with such events. The frequencies of these turbulent events have been assessed from wavelet analysis and found to concentrate in two zones that closely match predictions from empirical equations. Such a finding suggests that a combination and interaction of vortex shedding and wake flapping/changing length of the lee-side separation zone are the principal contributors to the turbulent flow field associated with such large alluvial sand dunes. Wavelet analysis provides insight upon the temporal and spatial evolution of these coherent flow structures, including information on the topology of dune-related turbulent flow structures. At the flow stage investigated, the turbulent flow events, and their associated high suspended sediment concentrations, are seen to grow with height above the bed until a threshold height (*ca* 0·45 flow depth) is reached, above which they begin to decay and dissipate.

Keywords Dune, flow, Rio Paraná, sediment transport, turbulence, wavelet analysis.

[1]Present address: Centre for Natural Hazard Research, Department of Earth Sciences, Simon Fraser University, Burnaby, BC, Canada V5A 1S6

INTRODUCTION

Turbulence is a fundamental property of river flows and is the principal driving force behind sediment transport (e.g. Babakaiff & Hickin, 1996; Kostaschuk, 2000; Best, 2005b). Although early research suggested that such turbulence was essentially random (e.g. Matthes, 1947; Clifford & French, 1993), it is now generally accepted that turbulence is organized, and related in part to coherent flow structures that are irregular, but repetitive, spatio-temporal flow patterns (e.g. Grass, 1971; Müller & Gyr, 1986; Roy *et al.*, 2004). These quasi-periodic motions are generated over both smooth and rough beds (e.g. Jackson, 1976; Villard & Kostaschuk, 1998), can cause orders of magnitude variations in sediment transport rates and are thought to be responsible for much of the vertical mixing and production of turbulent energy in rivers (Lapointe, 1992; Kostaschuk & Church, 1993; Best, 1996).

Research commencing in the late 1960s and early 1970s (Grass, 1971; Kline *et al.*, 1967; see reviews in Robinson, 1991 and Smith, 1996) identified the key characteristics of boundary layer turbulence generated over a smooth wall as being: (i) microturbulent 'bursts', which are relatively slow-moving packets of fluid that are sourced near the bed and ejected toward the flow surface ('ejections'); and (ii) inrushes of higher velocity fluid ('sweeps') from the overlying flow that, through mass and momentum continuity, must replace the fluid 'ejected' during a burst. Additionally, several researchers have observed that, at the river scale, the flow surface is often disturbed by circular patches of upwelling fluid, termed 'boils', that are thought to be the surface manifestation of vortices that originate near the bed, termed 'kolks' (e.g. Matthes, 1947; Jackson, 1976; Kostaschuk & Church, 1993; Bennett & Best, 1995; Kostaschuk & Villard, 1996a; Roy *et al.*, 2004; Best, 2005a,b). The origin of kolks and boils in large rivers has been attributed variously to boundary layer bursting (Jackson, 1976; Yalin, 1992) and processes related to form roughness, such as the generation of Kelvin–Helmholtz instabilities associated with shear layers (Müller & Gyr, 1986; Kostaschuk & Church, 1993; Bennett & Best, 1995; Best, 1996, 2005a; Venditti & Bennett, 2000; Yue *et al.*, 2005; Stoesser *et al.*, 2008) and shear-layer destabilization (Nezu & Nakagawa, 1993). Regardless of the actual mechanism, the entrainment and transfer of suspended sediment within these turbulent structures is an important geophysical process, and yet there is still an incomplete understanding of both how such turbulent structures originate, grow and dissipate and how they are linked quantitatively with suspended sediment concentration (SSC) and transport.

Another matter that has recently attracted significant interest is the relationship between dune geometry and sediment transport (e.g. Smith & McLean, 1977; Kostaschuk & Villard, 1996a; Carling *et al.*, 2000; Kostaschuk, 2000; Best & Kostaschuk, 2002; Best, 2005b; Parsons *et al.*, 2005). Contemporary dune models assume a highly asymmetric shape with a sharp crest and lee-side flow separation (c.f. Kostaschuk & Villard, 1996a; Best & Kostaschuk, 2002). Smith & McLean (1977) attributed the asymmetric shape of dunes in their study to the predominance of bed load transport. When flow strengths are low, sediment is transported primarily as bed load up the stoss side of the dune and avalanches down the lee side, maintaining an 'angle-of-repose' slope. Wilbers (2004), however, argues that the most common dunes in sand bed rivers have a gentle stoss side, often of only a few degrees, leading up to a crest that is gently curved to a 'brinkpoint' where the lee-side angle changes abruptly into the angle-of-repose slope. Wilbers (2004) contends that the size and shape of flow separation zones depends primarily on the height of the separation point (brinkpoint) and not on lee-side angle, as concluded by several authors (e.g. Johns *et al.*, 1993; Kostaschuk & Villard, 1996a; Best & Kostaschuk, 2002).

Several authors (e.g. McLean & Smith, 1979; Kostaschuk & Ilersich, 1995; Best & Kostaschuk, 2002) have demonstrated that steep-sided asymmetrical dunes may be rare in sand bed rivers where a higher proportion of sediment is transported in suspension. Increased suspended load transport can lead to deposition on the lee slope and in the trough, which results in lower lee slope angles and a progressive loss of permanent flow separation. The outcome is stoss-side and lee-side lengths that are more comparable in length, lower dune height/length ratios and lee-side slope angles that are much less than the angle-of-repose.

The purpose of this study is to investigate dune-related fluid turbulence by examining the coherence between time series of three-dimensional (3D) flow and sediment transport over the crest of a single large sand dune in the Río Paraná, Argentina. The present contribution has three objectives: (i) to quantify the 3D velocity and sediment concentrations associated with coherent flow structures generated by the dune; (ii) to determine the relationship between the streamwise horizontal velocity, vertical velocity and

SSC using phase-coherence cross-wavelet analysis; and (iii) to examine the spatio-temporal evolution of coherent flow structures using a series of stacked wavelet power spectra derived from the vertical profiles of suspended sediment.

METHODS AND ANALYSIS

Field study site

The present study was conducted on the Río Paraná, just upstream of its confluence with the Río Paraguay, NW Argentina (27°30′ S, 58°50′ W; Fig. 1). The mean annual discharge of the Río Paraná in this reach is *ca* 12 000 m^3 sec^{-1} (Orfeo & Stevaux, 2002). In the Río Paraná, summer floods and spring low water levels are common, although during the field season in the austral summer of 2004, the river experienced slightly lower flows than usual, with discharge during the time of survey being *ca* 11 000 m^3 sec^{-1}. At the study site, the Río Paraná is *ca* 2·5 km wide and between 5 and 12 m deep, and the flow was fully turbulent ($Re \approx 8 \times 10^6$) and subcritical ($Fr \approx 0{\cdot}11$).

Data collection

Flow and sediment transport data were collected from a small survey vessel on 9 March 2004, while a more extensive bathymetric survey was conducted from a second, larger, vessel. The survey strategy involved measurement of: (i) bathymetry using a RESON™ SeaBat® 8101 multibeam echo sounder (MBES; Reson, Slangerup, Denmark; see Parsons *et al.*, 2005); (ii) 3D flow velocity using a Teledyne RDInstruments® (Poway, CA, USA) RíoGrande 600 kHz acoustic Doppler current profiler (aDcp) with a bin spacing of 0·5 m; and (iii) SSC and particle size with a Sequoia® Scientific laser *in situ* scattering transmissometer (LISST; Sequoia Scientific, Bellevue, WA, USA).

The MBES, which uses 101 sonar beams that 'ping' to acoustically illuminate a swath of the riverbed 150° across track by 1·5° along track, was tied spatially and temporally to the aDcp and LISST data using a Leica Differential Global Positioning System (dGPS; Leica Geosystems, St. Gallen, Switzerland) in Real-Time Kinematic (RTK) mode, which resulted in a relative accuracy of ±0·02 m and ±0·03 m in the horizontal and vertical positions, respectively. Accuracy of the MBES is not affected by bed slope, since the MBES works along track and, depending on the grazing angle of the beam, both phase and amplitude returns are used in bottom detection. The aDcp was mounted to the side of the small survey vessel by means of a pivoting bracket, which allowed the instrument to be rotated into the water and held vertically in place during measurements. This arrangement allowed 3D velocity and acoustic backscatter intensity to be measured both from a stationary anchored position and while the vessel was moving. The LISST, which measures particle size based on principles of laser diffraction (Agrawal & Pottsmith, 2000), was attached to a boat-mounted winch on the small launch by means of a steel wire and data-transmitting cable, and was allowed to trail below the boat while moored at-a-point. Whilst moored at-a-point, using two anchors both fore and aft of

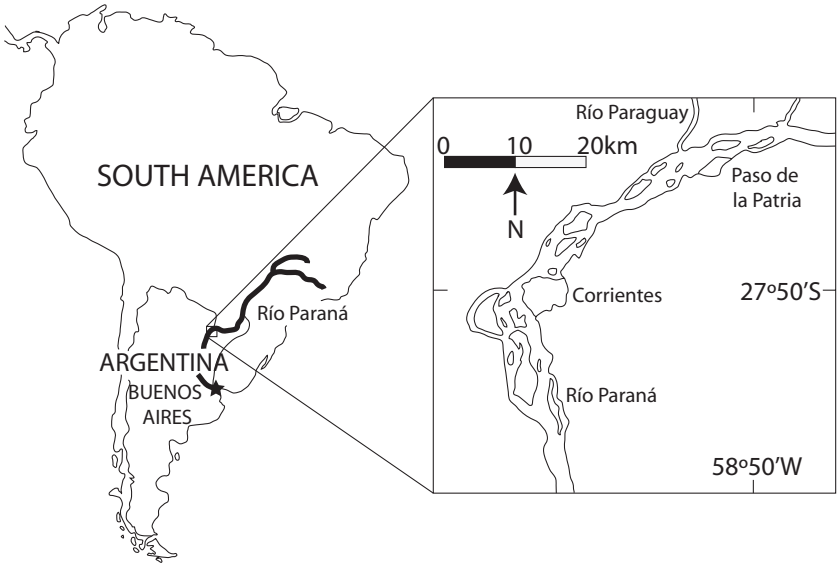

Fig. 1. Location map of the study area.

the vessel, the boat moved slowly in the cross-stream direction by up to *ca* 5 m, but did not migrate downstream. The MBES was mounted securely to the bow of the larger vessel that surveyed the entire dune field (see Parsons *et al.*, 2005 for details) and was also tied into the survey using a second RTK dGPS receiver. Finally, a series of bed sediment samples was collected and later sieved in the laboratory to determine the grain-size distribution of the bed material.

Data analysis

Sand suspension and plankton modelling

Plankton biomass in the Río Paraná is generally low relative to other parts of the World (Gomes & Miranda, 2001; Zalocar de Domitrovic, 2005). However, during the austral summer of 2004, plankton blooms in the Yacyretá Dam reservoir, *ca* 100 km upstream of the study site, were exceptionally high and contaminated some of the suspended sediment data generated by the LISST. In order to separate the signal from the plankton and suspended sediment, the Rouse sediment concentration profile (see Soulsby, 1997; Kostaschuk *et al.*, 2003) was used to estimate suspended bed-material concentrations throughout the water column. The model was applied using the observed, sieved size distributions obtained from the bed material grab samples. Once this process had been performed, the predicted relative contribution of each grain size was compared with the results from the LISST at each height in the vertical, in order to estimate the contributions of sediment and plankton. The methodology employed follows that outlined in Kostaschuk *et al.* (2003, 2004) and Soulsby (1997), and only an abridged description is given below.

Bed-material entrainment and suspension are related to the shear stress of the flow, τ_0, which can be expressed as a function of shear velocity, u_*:

$$\tau_0 = \rho u_*^2 \quad (1)$$

where ρ is the density of water. Total shear stress exerted by the flow is composed of the skin stress acting on sediment particles, τ_{0s}, the form stress produced by large bedforms, τ_{0f}, and the sediment transport stress caused by momentum transfer in particle entrainment, τ_{0t} (Soulsby, 1997):

$$\tau_0 = \tau_{0s} + \tau_{0f} + \tau_{0t} \quad (2)$$

Values of τ_{0t} are usually very small in natural flows.

Kostaschuk *et al.* (2004) compared aDcp-based estimates of shear stress using the 'law-of-the-wall', which relies on measurements of u_*, and models based on the quadratic stress equation, including those of Yalin (1992), Smith & McLean (1977) and van Rijn (1984, 1993). The quadratic stress equation is given as:

$$\tau_{0s} = \rho C_D \bar{u}^2 \quad (3)$$

where C_D is the drag coefficient and $\bar{u}$ is the mean flow spatially averaged over the entire dune. Kostaschuk *et al.* (2004) recommend use of the van Rijn quadratic stress model, and thus it was used in the present study (see van Rijn, 1984, 1993, for further details on model application). The van Rijn model estimated total τ_0 = 7·81 Pa and total u_* = 0·086 m sec^{-1} for the study dune.

Although the entrainment of sediment is a function of skin friction, diffusion of sediment into the water column is controlled by turbulence, which is reflected in the total stress (Soulsby, 1997). Sand suspension in a river can be considered to be a settling-diffusion problem where the settling of grains to the bed is counteracted by upward movement of grains due to turbulent diffusion (Soulsby, 1997; Kostaschuk *et al.*, 2003):

$$w_s C = -K_s \frac{dC}{dz} \quad (4)$$

where w_s is the grain settling velocity, C is the volume concentration of sand at height z above the bed and K_s is the eddy diffusivity of sediment. Several models have been proposed for solution of Eq. 4, including the power-law profile, the Rouse profile and the van Rijn profile (Soulsby, 1997). The power-law profile is obtained if eddy diffusivity is assumed to vary linearly with height, whilst if a parabolic profile is assumed, the Rouse profile is obtained. The van Rijn approach is recommended for use if strong density stratification caused by sediment is expected (Soulsby, 1997). Given the relatively low flow velocity and SSCs during the present surveys in the Río Paraná, the Rouse concentration profile is therefore used herein. The model was set up to predict the concentration of each grain size, assuming an unlimited supply of perfectly unimodal grains of that size, and was run five times, each for a different sieve-based grain size (e.g. d = 62, 125, 250, 500 and 1000 μm). Each concentration, Cz, was then multiplied by the percentage of bed material of that size, as determined by sieve analysis of bed grab samples.

Figure 2A compares predicted grain-size distributions in suspension to grain-size distributions measured *in situ* by the LISST. It is clear from the model that for heights > 2 m above the bed, and especially > 4 m above the bed, sediment > 250 μm is not suspended in any great quantity. Laser *in situ* scattering transmissometer rings 29 (median grain size 293 μm) through to 32 (462 μm) are coarser than 250 μm and thus probably reflect the contribution of plankton. Therefore, these rings are excluded from the analysis. However, these predictions are based on time-averaged

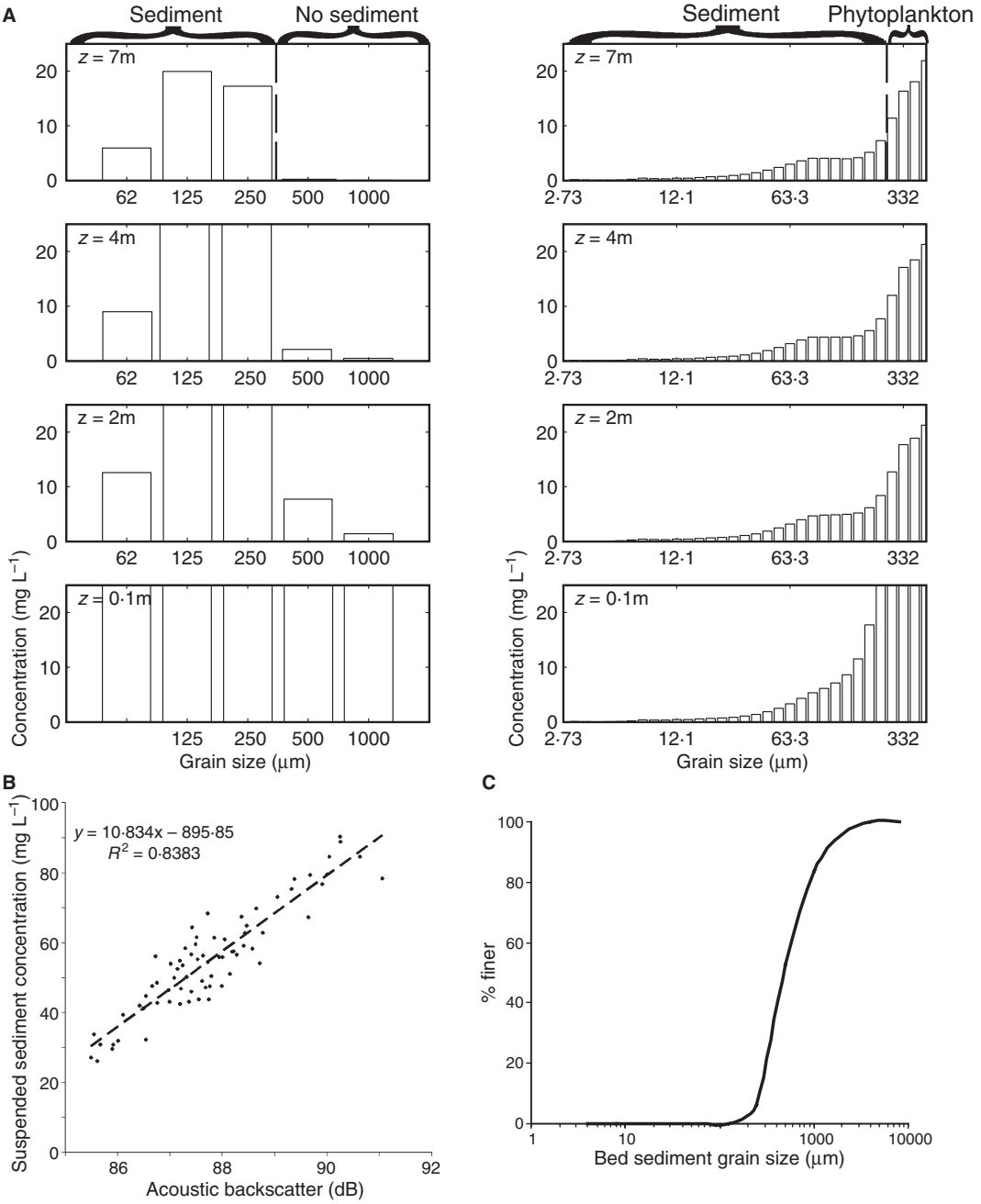

Fig. 2. (A) Grain-size distributions for various heights above the bed predicted by the Rouse profile and bed material composition (left) and data collected *in situ* with the laser *in situ* scattering transmissometer (LISST, right). From predicted distributions, it is clear that almost no sediment > 250 μm will be entrained under the flow conditions of this study. The measured distributions therefore reflect both sediment and plankton (i.e. > 250 μm). (B) Calibration curve of LISST-generated suspended sediment concentrations and acoustic backscatter from the aDcp. (C) A typical grain-size distribution obtained by sieving bed material collected from the dune field, Río Paraná.

values of shear stress, and they may not account for particularly strong events that suspend sand coarser than 250 μm, especially near the bed. A grain-size distribution with an abrupt cut-off at 250 μm is unrealistic in nature, especially in turbulent flows where strongly coherent flow structures would be expected to entrain especially large grains. Under the field conditions encountered, however, this avenue was the most unambiguous and most appropriate course of action for removing the significant influence of the plankton upon the grain-size distribution. In addition, the contributions of the plankton to the smaller size fractions remain undetected, but are assumed herein to be relatively constant given their lower density. Moreover, it is likely that much of the plankton was > 250 μm in diameter, as they were easily discernible in the field with the naked eye. The adjusted sediment concentrations from the LISST are similar to the values reported by Bonetto & Orfeo (1984) in the Río Paraná for the same time of year. These LISST-generated, at-a-point 'decontaminated' SSCs were then used to calibrate the acoustic backscatter from the aDcp (Fig. 2B, r^2 = 0·84; accounting also for the acoustic attenuation with depth, see Kostaschuk *et al.*, 2005). In order to estimate the full field SSCs (see Kostaschuk *et al.*, 2005 and Shugar, 2005 for further details), the calibration was performed on *ca* 60 sec samples from both the LISST and aDcp records. A typical sieve-generated grain-size distribution of bed sediment in the study reach of the Río Paraná is given in Fig. 2C.

Wavelet analysis

Although coherent flow structures are somewhat periodic, most studies of turbulent flow over dunes have not considered the effect of non-stationarity in the time series. As a result, this intermittency in a time series is often extremely difficult to analyse with traditional spectral methods such as the Fourier transform (e.g. Venditti & Bennett, 2000). Because of this difficulty, wavelet analysis has been used in the present study because the time series of both velocity and suspended sediment transport are likely to contain non-stationary features and vary intermittently over time (e.g. Kostaschuk & Church, 1993; Best, 2005a; b; Venditti & Bauer, 2005).

Wavelet transforms allow a signal to be decomposed into both time *and* frequency. The analysis is based upon wavelets that are localized in time (Farge, 1992) and are most easily understood when compared with the more commonly used Fourier transform. The Fourier transform decomposes a signal into a series of sinusoids and expresses the signal in terms of the frequency and power of its constituent waves, but *without* reference to when the frequencies occur. This observation therefore imposes the requirement that the underlying frequencies are constant in time, a condition not often met in turbulent time series. The wavelet transform decomposes a time series into a set of scaled and translated versions of wavelet functions, $\Psi(\eta)$. Thus, whereas a Fourier transform in the frequency domain yields a power value for each frequency, and is inherently non-local, wavelet analysis produces power values for a set of locations in time and for a range of frequencies, the latter being related to the scales of the wavelet function considered. The wavelet transform is termed 'continuous' where the transform is calculated for all scales and positions in time and 'discrete' where the transform operates on discrete dyadic scales and positions in time. The continuous wavelet transform of a discrete time series, x_n, is defined as the convolution of x_n with a scaled (by s) and translated (by a localized time index n) version of normalized $\Psi(\eta)$:

$$C_n^X(s) = \sum_{n'=0}^{N-1} x_{n'} \Psi^* \left[\frac{(n'-n)}{s} \right] \delta t \qquad (5)$$

where the asterisk (*) indicates the complex conjugate, N is the number of points in the data series and δt is the time step used in the analysis. Thus, the continuous wavelet transform describes the fit of the wavelet function for all time periods and all frequencies, although the values of the wavelet power spectrum represent the magnitude of the variance in the series at a given wavelet scale and location in time. It is possible to integrate the spectrum through time or scale, the former yielding a power spectrum that is equivalent to a Fourier power spectrum, but with the added benefit of revealing scales of non-stationary variability not identified in a conventional Fourier analysis. Additionally, since Fourier analysis assesses the global fit of a sinusoid of time-constant scale at all scales, for numerical reasons it may not yield the same results as the wavelet power spectrum, which is based upon the fit of a time-varying wavelet. However, integration through scale within wavelet analysis produces a power spectrum that identifies when in the series the total power (i.e. wavelet fit) is greatest (e.g. Bjerkås, 2006).

Various mother wavelets of different shapes and styles can be applied in the analysis and, although

this choice can be arbitrary, the type of mother wavelet applied should not have a significant bearing on the qualitative results obtained. One criticism often made of wavelet analysis is the seemingly arbitrary choice of the wavelet function used. Torrence & Compo (1998) have made an effort to standardize the choice of wavelet function by classifying wavelets based on four factors: (i) orthogonal or non-orthogonal; (ii) real or complex; (iii) width; and (iv) shape. With orthogonal wavelets, the number of convolutions at each scale is proportional to the width of the wavelet base at that scale which produces a wavelet spectrum with discrete blocks of wavelet power (Torrence & Compo, 1998); they can only be used for discrete wavelet transforms although they produce the most compact representation of the signal. Non-orthogonal wavelets are more appropriate for time series analysis because they allow for continuous variation in wavelet power. Complex wavelet functions return information on both amplitude and phase and are best suited for capturing oscillatory behaviour, whereas real wavelets return only a single coefficient and are useful in isolating single peaks. The resolution of a wavelet function is determined by the balance between width in real space and width in Fourier space where a narrow (in time) function will have good time resolution but poor frequency resolution and vice versa (Torrence & Compo, 1998). It is often argued that the shape of the mother wavelet should share characteristics of the analysed signal. Tennekes & Lumley (1972) provide a schematic diagram for a characteristic turbulent 'eddy', which they argue provides the most suitable elementary decomposition of turbulent energy. Liandrat & Moret-Bailly (1990) suggest that the shape of the eddy given by Tennekes & Lumley (1972) is remarkably similar to the Morlet wavelet, and this wavelet is therefore utilized herein and, as shown below, provides a convincing fit to the data collected.

For any time series with equal temporal increments indexed by n, a wavelet function, $\Psi(\eta)$, that depends on a non-dimensional 'time' parameter, η, can be applied. The Morlet wavelet used herein consists of a plane wave modulated by a Gaussian envelope:

$$\Psi(\eta) = \pi^{-1/4} e^{i\omega_0 \eta} e^{-\eta^2/2} \quad (6)$$

where ω_0 is the dimensionless frequency and i is the imaginary part of a complex number (Farge, 1992; Torrence & Compo, 1998; Lafrenière & Sharp, 2003). The Gaussian envelope $(-\eta^2/2)$ localizes the wavelet in time (Maraun & Kurths, 2004). When comparing two series, X and Y, the local wavelet cross-spectrum (or covariance) of the two series can be determined from:

$$W_n^{XY}(s) = C_n^X(s) C_n^{Y^*}(s) \quad (7)$$

where $C_n^{Y^*}(s)$ is the complex conjugate of $C_n^Y(s)$. The cross-wavelet power is then defined as $\left|W_n^{XY}(s)\right|$. The transform can then be divided into the real part, $\Re\{W_n(s)\}$, and the imaginary part, $\Im\{W_n(s)\}$, or amplitude $|W_n(s)|$ and phase ϕ_n^m:

$$\phi_n^m = \tan^{-1} \frac{\Im\left[C_n^m(s)\right]}{\Re\left[C_n^m(s)\right]} \quad (8)$$

It thus follows that the wavelet and phase coherence can also be determined (e.g. Torrence & Compo, 1998; Lane, 2007).

Traditionally, Fourier coherency has been used to identify frequency bands where two time series are related. The inability of traditional Fourier decompositions to keep locality present in the signal, however, means that important information can be lost in the time–frequency transformation. Torrence & Webster (1999) argue that wavelet phase coherency provides a more useful result as both frequency bands and time intervals of the covariation of the series can be examined. In qualitative terms, the wavelet cross-spectrum identifies where in the time series, and over what scale (frequency), the agreement is good. More specifically, phase coherence analysis allows examination of whether regions with a large common power in time–frequency space have a consistent phase relationship and therefore are suggestive of linkages and possible causality between the series. The phase is given in degrees (−180° to 180°), where values of −180° and 180° indicate that the two series are completely out-of-phase and 0° indicates that they are perfectly in-phase. The level of coherence can be tested for significance using standard procedures, and all wavelet spectra shown in this study are significant at 95% confidence limits, as tested relative to a white noise spectrum. Torrence & Compo (1998) and Lane (2007) provide more detailed explanations of the analytical techniques utilized herein.

RESULTS AND DISCUSSION

Dune morphology and mean flow

Figure 3 shows the bathymetry of the dune field examined in this study as revealed from the MBES survey. The dunes generally have a 3D

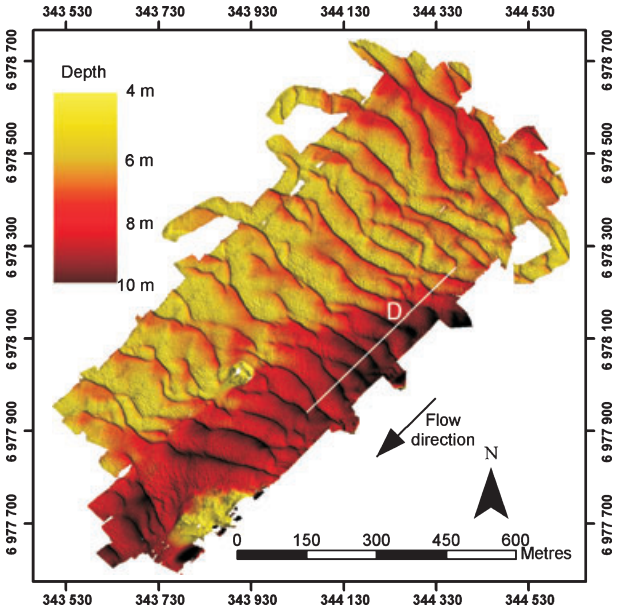

Fig. 3. Bathymetric map of the entire dune field obtained using a multibeam echo sounder. The study dune is marked by a white 'D' and the detailed profile from the streamwise transect line (solid white line) is shown in Fig. 4 (see Parsons *et al.*, 2005).

shape, with various degrees of crestline sinuosity, including crestline discontinuities and bifurcations (Parsons *et al.*, 2005). Within the survey area, individual dunes range from 1 to 2·5 m in height with wavelengths between 45 and 85 m. Flow depth increases in the south-west corner of the survey area, with a corresponding increase in dune size. The majority of dunes are asymmetric in downstream profile, with lee slope angles typically *ca* 8·5° to 18°, although lee slopes of up to 22° are present (Fig. 4). Dune stoss slopes are much shallower, typically *ca* 1·5° to 2·5°. The dune chosen for detailed study herein (Fig. 4) was asymmetric in downstream profile, with a distinct crestal brinkpoint resulting in an upper lee-side slope of 10·3° and a lower lee-side slope of 21·8°. The stoss slope had an angle of *ca* 3°. The dune was 45 m long and 2·05 m in height, with superimposed bedforms on the study dune being concentrated on the upper stoss slope and crestal region. Dune heights are of the same order as those measured by Amsler & Garcia (1997) and Amsler *et al.* (2003) in the middle reach of the Río Paraná.

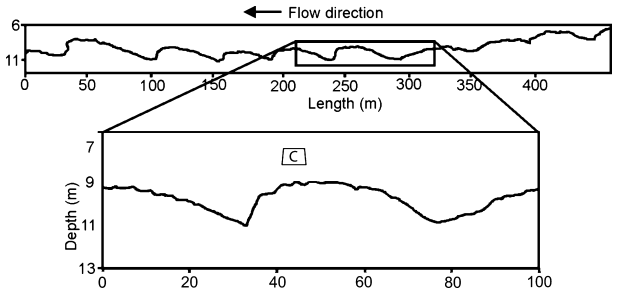

Fig. 4. Profile of bed morphology along the streamwise transect line shown on Fig. 3, with the study dune shown in detail. Location and size of bottom-most aDcp bin, labelled 'C', is shown over the crest. Vertical exaggeration is 10×.

Flow velocities measured with the aDcp along a streamwise transect (Figs 3 and 4) through the dune field (Fig. 5) show some evidence for flow reversal ($-U$ values) in the dune troughs, although it is difficult, due to beam spreading and the non-uniformity of flow within the aDcp sampling volumes near the bed, for the aDcp to fully resolve flow velocity in the lee-side separation/deceleration zone (e.g. Kostaschuk *et al.*, 2004; Parsons *et al.*, 2005). The results indicate topographic forcing of the flow field (e.g. Nelson *et al.*, 1993; McLean *et al.*, 1994; Bennett & Best, 1995; Kostaschuk & Villard, 1996b; Best *et al.*, 2001; Best & Kostaschuk, 2002; Kostaschuk *et al.*, 2004; Best, 2005b; Parsons *et al.*, 2005) which causes higher, positive, streamwise flow velocity ($+U$) and upward vertical velocity ($+W$) over dune crests and lower ($+U$), or reversed ($-U$), streamwise flow velocity and downward vertical velocity ($-W$) over the troughs (Fig. 5).

Velocity time series

Time series of streamwise velocities obtained while the boat was anchored at-a-point over the crest ($\bar{u}$ = 0·98 m sec^{-1}, σ = 0·04 m sec^{-1}) of the dune are given in Fig. 6. The streamwise veloc-

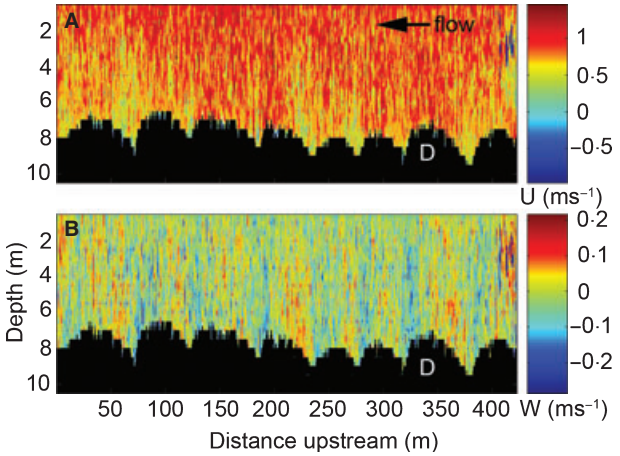

Fig. 5. Transect showing (A) streamwise flow velocity and (B) vertical flow velocity along the dashed profile in Fig. 3. The study dune is at 'D'.

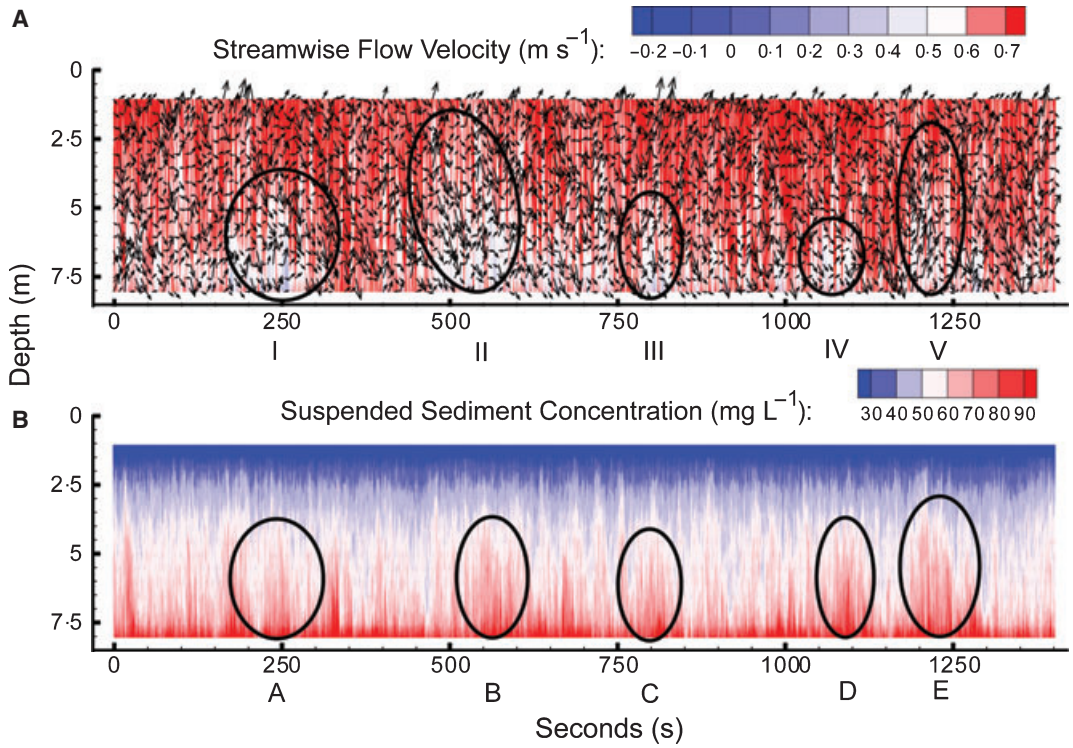

Fig. 6. Time series of: (A) the streamwise component of flow velocity with flow vectors representing vertical flow over the crest; (B) the calibrated acoustic backscatter (suspended sediment concentration) over the crest.

ity is plotted with 0·35 m sec^{-1} subtracted from the velocities: the velocity field thus appears as seen travelling at 0·64$\bar{u}$, and is used to better educe the coherent structures present (see Adrian *et al.*, 2000). In several instances over the dune crest, flow structures with relatively low horizontal velocity alternate with faster moving flow (Fig. 6A). These structures are manifested by fluid with a lower streamwise velocity being recorded first near the flow surface before being detected closer to the bed as the structure propagates downstream past the anchor station over the dune crest. Four example structures are highlighted in Fig. 6A. Between *ca* 150 and 275 sec (circled and labelled 'I', Fig. 6A), a body of low streamwise velocity fluid moves past the anchor station over the crest. Immediately following this, higher velocity fluid occurs throughout the water column between *ca* 300 and 400 sec. Also highlighted on Fig. 6A are similar events between 450 and 625 sec, between *ca* 775 and 850 sec, and again between 1040 and 1125 sec (labelled 'II' to 'IV', respectively, Fig. 6A) that advect over the dune crest. At *ca* 1175 sec, a fifth lower-velocity structure is circled, which continues for *ca* 100 sec (labelled 'V', Fig. 6A).

Some of the coherent flow structures detected in this study are most probably generated by dunes upstream of the study dune, which then propagate downstream and past the measurement profile at the dune crest. Flow vectors superimposed on the streamwise velocities in Fig. 6 illustrate the cyclic pattern of upwelling and downwelling fluid over the dune crest. Periods of downwelling alternate with periods of upwelling (Fig. 6A), especially in the bottom half of the flow field, where upwelling is observed between *ca* 175 and 250 sec, whereas between 250 and 400 sec the flow vectors indicate downwelling. This alternating pattern continues throughout the time series, with major upwellings observed from *ca* 400 to 450, 525 to 550, 700 to 850 and 1100 to 1275 sec and downwellings from 450 to 525, 825 to 900, 1125 to 1175 and between 1300 and 1350 sec.

Suspended sediment time series

Time series of SSC calibrated from the aDcp backscatter collected over the dune crest (Fig. 6B) reveal several pulses of sediment erupting from the bed over the crest, although most do not penetrate very high into the overlying flow.

Particularly strong periods of increased suspended sediment are recorded from *ca* 150 to 275, 500 to 600, 775 to 850, 1000 to 1150 and 1175 to 1300 sec (labels 'A' to 'E', Fig. 6B).

The patterns of sediment suspension reported here are similar to those obtained in earlier numerical, flume and field studies (e.g. Johns *et al.*, 1990, 1993; Kostaschuk & Villard, 1996b, 1999; Carling *et al.*, 2000; Kostaschuk, 2000; Williams *et al.*, 2003), with relatively homogenous, low concentrations of sand characterizing the upper half of flow over dunes, and higher, more variable, sand concentrations being present in the lower half of the flow. For example, Kostaschuk & Villard (1999) demonstrate a 10-fold decrease in time-averaged sediment concentration, relative to near-bed conditions, throughout the water column over dunes in the Fraser Estuary, Canada, and Johns *et al.* (1990) report a similar concentration gradient over modelled sandwaves.

Velocity and suspended sediment interactions

Phase coherence spectra of flow velocity and suspended sediment over the dune crest are given in Fig. 7. The phase coherence wavelet plots illustrate several important characteristics of flow and sediment transport over dunes, including inverse correlations (phase values approaching −180° and 180°) between streamwise and vertical flow velocity and between streamwise velocity and SSC, as well as a positive correlation (phase values *ca* 0) between vertical velocity and SSC.

The cross-wavelet power spectrum (Fig. 7A) of streamwise and vertical flow velocity over the dune crest shows a strong phase disagreement, or inverse correlation, between medium-frequency (defined herein as having a period between *ca* 50 and 100 sec) and low-frequency (period *ca* >100 sec) events. The equivalent time series (Fig. 6A) shows regions of low streamwise veloc-

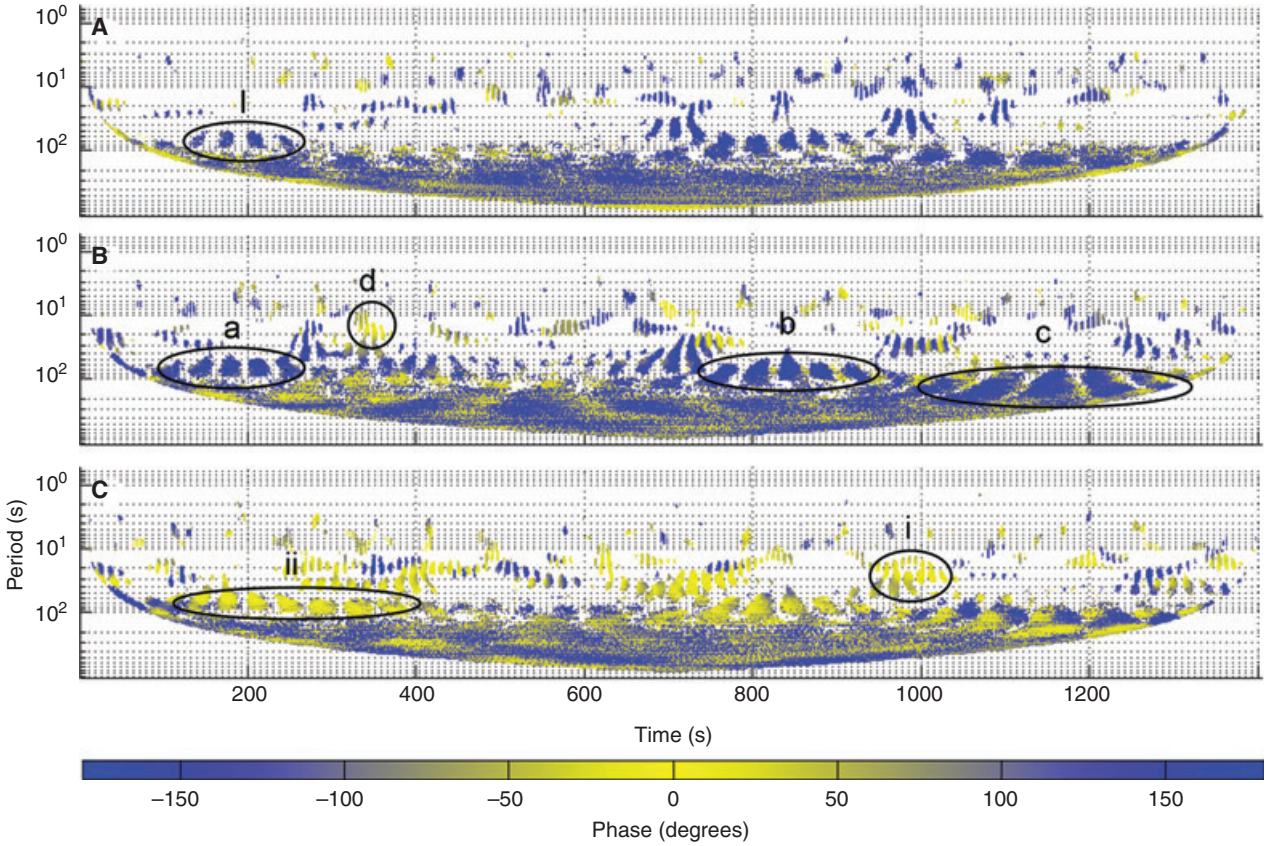

Fig. 7. Phase coherence wavelet spectrum of: (A) streamwise and vertical velocity; (B) streamwise velocity and calibrated suspended sediment concentration (SSC); and (C) vertical velocity and SSC, 3 m above the dune crest. Circled in (A) is a series of out-of-phase structures (labelled 'I'). Circled in (B) are three examples of out-of-phase structures (labelled 'a' to 'c') and a group of in-phase structures (labelled 'd'). Circled in (C) are two groups of in-phase structures (labelled 'i' and 'ii'), the latter being remarkably extensive. All circled regions are discussed in the text.

ity fluid matching well with regions of upwelling flow and vice versa, corroborating the phase pattern observed. For example, between 150 and *ca* 250 sec in the upper half of the flow (label 'I', Fig. 6A), an inrush of faster moving fluid from above replaces the upwelling flow in the lower half of the flow. The events from 150 to 250 sec are clearly visible in the phase coherence plot at a period of between 50 and 90 sec (label 'I', Fig. 7A). This inverse correlation between lower than average streamwise velocity and positive vertical velocity is expected for situations where the Reynolds stress is positive, as is the case here.

Figure 7B shows streamwise velocity to be strongly out-of-phase with the SSC above the dune crest in a pattern similar to Fig. 7A. Medium-frequency structures (periods between *ca* 50 and 100 sec), as well as low-frequency structures (periods between *ca* 150 and 350 sec), are strongly out-of-phase and common throughout the first 1000 sec of the time series (for example, between 100 and 250 sec, and from 750 to 950 sec, at a period ranging from 50 to 90 sec; labels 'a' and 'b', respectively, Fig. 7B). The remainder of the time series is characterized by strongly out-of-phase regions at periods ranging from 70 to *ca* 280 sec (e.g. label 'c', Fig. 7B). Several in-phase structures are present in the time series between 250 and 600 sec with a period ranging between *ca* 10 and 100 sec. For example, a group of in-phase structures with a period between 8 and 30 sec are observed between 325 and 375 sec in the series (label 'd', Fig. 7B). In addition, many of the higher frequency structures throughout the series are in-phase.

The phase coherence wavelet power spectrum of vertical velocity and calibrated SSC at 3 m over the dune crest (Fig. 7C) is similar to Fig. 7B, although SSC is noticeably more in-phase with vertical velocity than streamwise velocity. In-phase structures with periods *ca* >50 sec dominate the time series with regions possessing phase values either greater than 100° or less than −100° phase being relatively rare. Higher frequency (period <50 sec) and mostly in-phase structures interact intermittently throughout much of the time series and appear to occur in clusters of events (for example, from 950 to 1025 sec at periods ranging from 10 to 50 sec, label 'i', Fig. 7C). The edges of lower frequency packets (period *ca* >100 sec) are difficult to delineate on account of the low contrast in phase. In-phase structures with periods ranging from 10 to *ca* 130 sec are typical throughout the length of the series (for example, between 100 and 400 sec at periods between 40 and 100 sec, label 'ii', Fig. 7C).

The strongly out-of-phase coherence between streamwise flow velocity and SSC suggests that the two variables are inversely correlated, such that lower streamwise velocities are coupled with increased SSCs. This interpretation is supported by the equivalent time series of streamwise velocity and SSC (for example, Fig. 6A and B). Furthermore, Nelson & Smith (1989) reason that at low Froude numbers, boundary shear stress tends to lag behind sediment flux, as a result of sediment inertia effects, gravitational effects and suspended load transport. Conversely, the strongly in-phase coherence between vertical velocity and SSC suggests that SSC is higher in flows directed towards the flow surface. These results agree with and confirm the findings of previous work (e.g. Matthes, 1947; Jackson, 1976; Lapointe, 1992; Kostaschuk & Church, 1993; Babakaiff & Hickin, 1996; Kostaschuk & Villard, 1996a; Schmeeckle *et al.*, 1999; Shimizu *et al.*, 1999; Best, 2005a,b) on the effect of coherent turbulent flow structures on sand suspension. Both the highly out-of-phase coherence between streamwise flow velocity and SSC, and the highly in-phase coherence between vertical velocity and SSC, are attributed to ejections of fluid moving from near the bed into the outer flow, which have a lower streamwise velocity than the average and a higher than average vertical velocity. Inrushes of fluid back towards the bed tend to be characterized by higher than average streamwise velocities, negative (i.e. downwards) vertical velocities and lower concentrations of sand in suspension.

Separation zone lengths and turbulence frequencies

Empirically-derived relationships for the reattachment length of the flow separation zone as a function of step height have been proposed by numerous authors (generally, x_r/h *ca* 4 to 8, where x_r is the reattachment length and h is the step height (Engel, 1981; Nelson & Smith, 1989; Bennett & Best, 1995; Best & Kostaschuk, 2002; Wilbers, 2004; Yue *et al.*, 2005; Coleman *et al.*, 2006; Schatz & Herrmann, 2006). For subaqueous dunes, Bennett & Best (1995) suggest a reattachment length of 4·25 h, which is in good agreement with that proposed by Engel (1981) and Coleman *et al.* (2006), and slightly lower than that suggested by the modelling results of Yue *et al.* (2005). Schmeeckle *et al.* (1999) note that the

Table 1. Predicted turbulence periodicities* based on a range of reattachment lengths.

	Schatz & Herrmann, (2006)† $x_r = (A\alpha + B)\Delta\alpha/\alpha$	Bennett & Best (1995) $x_r = 4{\cdot}25h$	Carling *et al.* (2000) $x_r = 8{\cdot}3h$	Wilbers (2004) $x_r = h/\tan(10°)$	No x_r
Driver *et al.*, (1987): $P_v = x_r/0{\cdot}6\bar{u}$	24	16	30	21	
Simpson (1989): $P_v \approx x_r/0{\cdot}8U_o$	17	11	22	15	
Simpson (1989): $P_w < x_r/0{\cdot}1U_o$	137	89	173	119	
Strouhal Law (e.g. Kostaschuk, 2000): $P_s = 2\pi\delta/U_s$					45
Itakura & Kishi (1980): $P_d = h/0 \cdot 14\bar{u}$					16

*Where P_v is the vortex shedding periodicity, P_w is the wake flapping periodicity, P_s is the Strouhal periodicity, P_d is the dune periodicity, A is 0·22/° (see Schatz & Herrmann, 2006), α is the lower brink angle (21·8°), B is a constant (6·473, see Schatz & Herrmann, 2006), Δ is the lower brink height (1·6 m), h is the dune height (2·05 m), δ is the flow depth (7·5 m at dune crest), $\bar{u}$ is the mean velocity over the dune (*ca* 0·93 m sec^{-1}), U_o is the mean velocity upstream of the step (*ca* 0·98 m sec^{-1}) and U_s is the free stream velocity (1·04 m sec^{-1}).
†Schatz & Herrmann (2006) point out that their x_r calculation is for an isolated dune and the separation length of the dune in a dune field is *ca* 25% smaller. The values computed in Table 1 are therefore adjusted for a dune field.

reattachment point is extremely difficult to pinpoint except in a time-mean sense, and Carling *et al.* (2000) caution that reattached flow may not fully recover its 'upstream' hydraulic and sediment transport characteristics within the expected length of reattachment.

There seems to be general agreement (e.g. Nezu & Nakagawa, 1993; Kostaschuk, 2000) that eddies generated by dunes or negative steps originate in the separation zone/shear at two dominant frequencies. The Strouhal law discussed by Levi (1983, 1991) describes the frequency of shear-layer generated turbulent structures, although Itakura & Kishi (1980) proposed an empirical, flume-based relationship for the frequency of turbulent structures generated by dunes. Simpson (1989) proposed scaling relations for the frequencies of: (i) movement in the position of the point of flow reattachment ('vortex shedding'), f_v; and (ii) wake-flapping, f_w, associated with flow separation over a negative step, which offer possible explanations for the overall turbulence signature observed over the dune studied herein. Driver *et al.* (1987) present a similar vortex shedding relation to that of Simpson (1989). Table 1 provides a compilation of turbulence frequencies over the current study dune as predicted by several of these empirical relationships.

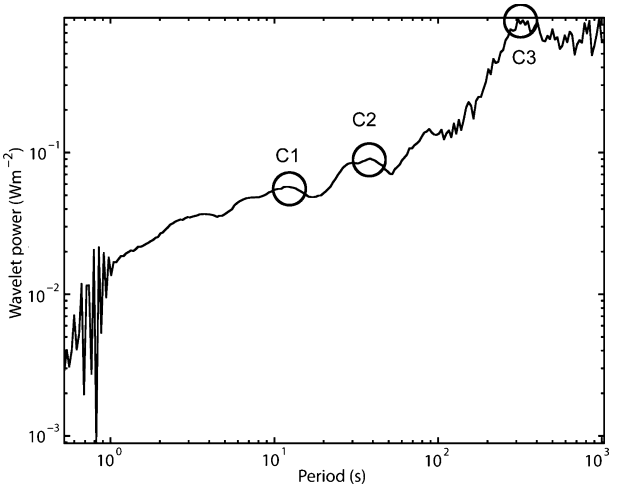

Fig. 8. Time-integrated wavelet power spectra of streamwise velocity 1 m above the dune crest. The peak at C1, with a period of 12 sec, has a wavelet power of 0·06 W m^{-2}; the peak at C2 has similar wavelet power (0·09 W m^{-2}) and lower frequency (period of 40 sec), while the lowest frequency peak, C3, has a wavelet power of *ca* 0·88 W m^{-2} and long period (307 sec).

A plot of time-integrated wavelet power (Fig. 8) from the near-bed streamwise velocity record over the dune crest provides field evidence to test the relationships proposed by Driver *et al.* (1987), Simpson (1989), Itakura & Kishi (1980) and the widely-cited Strouhal law. The spectrum shows a generally increasing trend in power with increasing period, as expected since the larger coherent flow structures contain more energy. Superimposed on this general trend is a series of peaks that are interpreted as representing the dominant turbulent frequencies generated by the bedforms. At 1 m above the dune crest, three peaks are obvious (labelled C1, C2 and C3, Fig. 8). Peak C1 has a period of 12 sec (wavelet power 0·06 W m^{-2}) and is consistent with the vortex

shedding frequencies predicted by Driver *et al.* (1987) and Simpson (1989) (16, 11 and 15 sec, respectively) using the reattachment length-scale of Bennett & Best (1995) and Wilbers (2004). The relationship of Itakura & Kishi (1980) also provides an excellent fit to the data (16 sec). The Schatz & Herrmann (2006) reattachment length-scale also provides a reasonable fit, although not as good as the length-scale of Bennett & Best (1995), possibly due to the former being derived for subaerial dunes. The reattachment length-scale proposed by Carling *et al.* (2000) is also a reasonable predictor but suggests less-frequent turbulence generation than that observed here. Peak C2 has a period of 40 sec (0·09 W m^{-2}) that is consistent with the Strouhal law prediction of a 45 sec period. Peak C3 has a period of 307 sec (0·88 W m^{-2}), which is significantly longer than predicted by any of the equations in Table 1. At periods longer than *ca* 300 sec, wavelet power is relatively consistent, suggesting that no single mechanism of turbulence generation is operating at these lower frequencies. With this in mind, it is possible that long-term, river-width scale events are contributing to the energy recorded over the dune crest. Alternatively, the lowest frequency structures may represent fragments of large coherent flow structures that have been generated by dunes much further upstream that are advecting downstream, which then interact with flow over the study dune. Only the largest of these flow structures would survive propagation downstream and would therefore contribute to this lower frequency portion of the spectra. This picture of flow structure is similar to that envisaged by Nelson & Smith (1989), with stacked wakes showing the presence of flow structures originating from upstream bedforms. Another plausible explanation is that the very low-frequency wavelet power is simply an artefact of the wavelet analysis, because wavelets as well as their Fourier counterparts must fit low-frequency waves to large but rare events, even when the large events last for a much shorter time. Further work is required at a range of sites to fully investigate and quantify these lower frequencies.

Nezu & Nakagawa (1993) describe wake flapping as resulting from the periodic entrainment of ambient water into the separation zone. Driver *et al.* (1987) note that low-frequency wake flapping contributes relatively little to overall turbulent energy and probably does not contribute much to turbulence generation, with most of the turbulent energy coming from vortex shedding. Driver *et al.* (1987) suggest that, although contributing little to turbulence, wake flapping may be a significant influence on the separation process, especially in flows where flow separation is sensitive to small disturbances. In the present study, however, turbulence frequencies attributed to wake flapping contribute more to the total energy than vortex shedding. Kostaschuk & Church (1993) used a current meter and acoustic profiler to quantify turbulent frequencies over dunes of similar size to the present study, and their flow records indicated a very regular motion with a period *ca* 11 sec, whereas the acoustic profiler produced a frequency distribution with a mean of 49 sec. Kostaschuk & Church (1993) attributed the current meter-measured periodicities to eddy shedding from the bed. Their 'acoustic kolks' represent only events sufficiently powerful to suspend significant quantities of sediment. Although Kostaschuk & Church (1993) compared their observed turbulence frequencies with those predicted by the Strouhal law, they suggested that free stream velocity may not be the best parameter to use in the calculation.

Venditti & Bauer (2005) point out that confusion persists regarding the Strouhal number because several candidates exist for use as a characteristic length-scale, including boundary layer thickness, dune height, flow depth and reattachment length. Although the approach is reasonable in simple bed configurations, Best (1993) warns that the predictive capacity of the Strouhal law may be premature in natural geophysical flows where particles may be poorly sorted, different size eddies might be generated from the same obstacle, and vortex pairing, tearing and amalgamation might significantly influence the size and frequency of eddies. Bennett & Best (1995) reason that although high-magnitude ejection events are capable of transporting more and coarser sediment, their frequency will differ from that predicted using the Strouhal law. Thus, five factors complicate the interpretation of the results presented herein when using the relationships proposed by Simpson (1989) and Driver *et al.* (1987).

Firstly, the frequency predictions of both Simpson (1989) and Driver *et al.* (1987) were derived for a simple, 90°, 2D, backward-facing step, and not dunes with a complex 3D morphology and much lower lee-side slope angles. Parsons *et al.* (2005) found that irregular crestline shapes of dunes in the Río Paraná produced smaller regions of lee-side flow separation (lower x_r) compared with straight-crested dunes, a result also found in

the laboratory experiments of Venditti (2003). Smaller regions of flow separation would thus result in lower eddy shedding frequencies than would be expected from relationships based on straight-crested steps. Secondly, the equations presented by Driver *et al.* (1987) are based on laboratory work that investigated a subaerial step, not a subaqueous dune and, therefore, this may not represent flow patterns in alluvial channels. Thirdly, the flow over alluvial dunes may be more 3D than assumed in 2D models, with flow going around an obstacle rather than just over it (Carling *et al.*, 2000; Maddux *et al.*, 2003; Parsons *et al.*, 2005). Additionally, the influence of variable asymmetric stoss-side profiles and composite lee-side slopes on the generation of dune-related turbulence is poorly understood. The study dune investigated herein, and indeed most alluvial dunes, have a composite lee-side slope with a gently sloping upper lee slope and a downstream, steeper lower lee slope. For example, the dune studied herein has an upper lee slope of 10·3° and a lower lee side of 21·8°. Both of these lee-side slope angles exceed the value of 10° suggested by Wilbers (2004) for the onset of flow separation, resulting in the possibility of two separate, or interacting, separation zones (see Fernandez *et al.*, 2006) that may generate coherent flow structures at different frequencies. Similarly, coherent flow structures from upstream dunes probably are advecting through the aDcp sensing volume over the study dune and are thus contributing to the total energy measured.

Fourthly, the superimposed small bedforms near the dune crest are also likely to generate coherent flow structures, and the interaction of bedforms may radically influence the flow structure at the crest and downstream, as recently reported by Fernandez *et al. (*2006). If coherent flow structures scale with bedform height (i.e. through the step height and reattachment length), then smaller superimposed bedforms would contribute to the higher frequency portion of the spectra.

Finally, it should be remembered that the beam spread of the aDcp (20° along each beam) affects the size of coherent flow structures that can be resolved at different heights above the bed (see Figs 9 and 10). As the measurement volume of a surface-deployed aDcp increases with distance below the surface, it is possible that only larger structures may be resolved in the near-bed region. However, there is a clear non-linear decrease in the scale of flow structure (both spatial and wavelet power) with increasing height above the bed, with many near-bed structures decaying rapidly above a threshold height of *ca* 0·45 flow depth (see Figs 9 and 10). This effect suggests that the observed evolution is not an artefact of aDcp beam-spreading but represents a real physical phenomenon. Additionally, the reasonable agreement between the predicted and measured frequencies discussed above suggests that most of the packets of wavelet power may be generated by the processes discussed by Simpson (1989). These findings are also similar to the previous work concerning flow over dunes by Kostaschuk (2000), who suggested that turbulence production associated with the separation zones of dunes in the Fraser River was governed, in part, by the evolution and interaction of flow structures associated with vortex shedding and wake flapping.

Faced with local non-stationarity in long velocity time series over dunes, Venditti & Bauer (2005) estimated the expected recurrence of turbulent events by applying the frequency relationships suggested by Simpson (1989) and split their time series accordingly. The Fourier transforms used by Venditti & Bauer (2005) demonstrated subdued and relatively featureless velocity co-spectra over dune crests, with much greater variance and a dominant spectral peak in the trough. Furthermore, Venditti & Bauer (2005) found a shift in frequency of the vertical velocity at the transition between the dune crest and lee, and suggested that eddy stretching and elongation by the mean flow may be responsible, although these authors also highlighted the possibility of the presence of two sets of oscillations in the flow. However, Venditti & Bauer (2005) conceded that, in their case, spectral analysis did not allow observation of intermittent wake flapping, or even observation of two independent sets of oscillations.

Spatio-temporal evolution of coherent flow structures

A vertical stack of wavelet plots of SSC, derived from calibrated aDcp backscatter records at different heights above the dune crest for the time series, illustrates the interaction and evolution of the coherent flow structures as they rise away from the bed and advect downstream (Figs 9 and 10). This stack of plots can be used to outline a conceptual model for the morphology of these large-scale turbulent structures that are associated with sand dunes. Overall, the number, size, period and power of the wavelet packets decrease with height above the bed (as circled in Fig. 9,

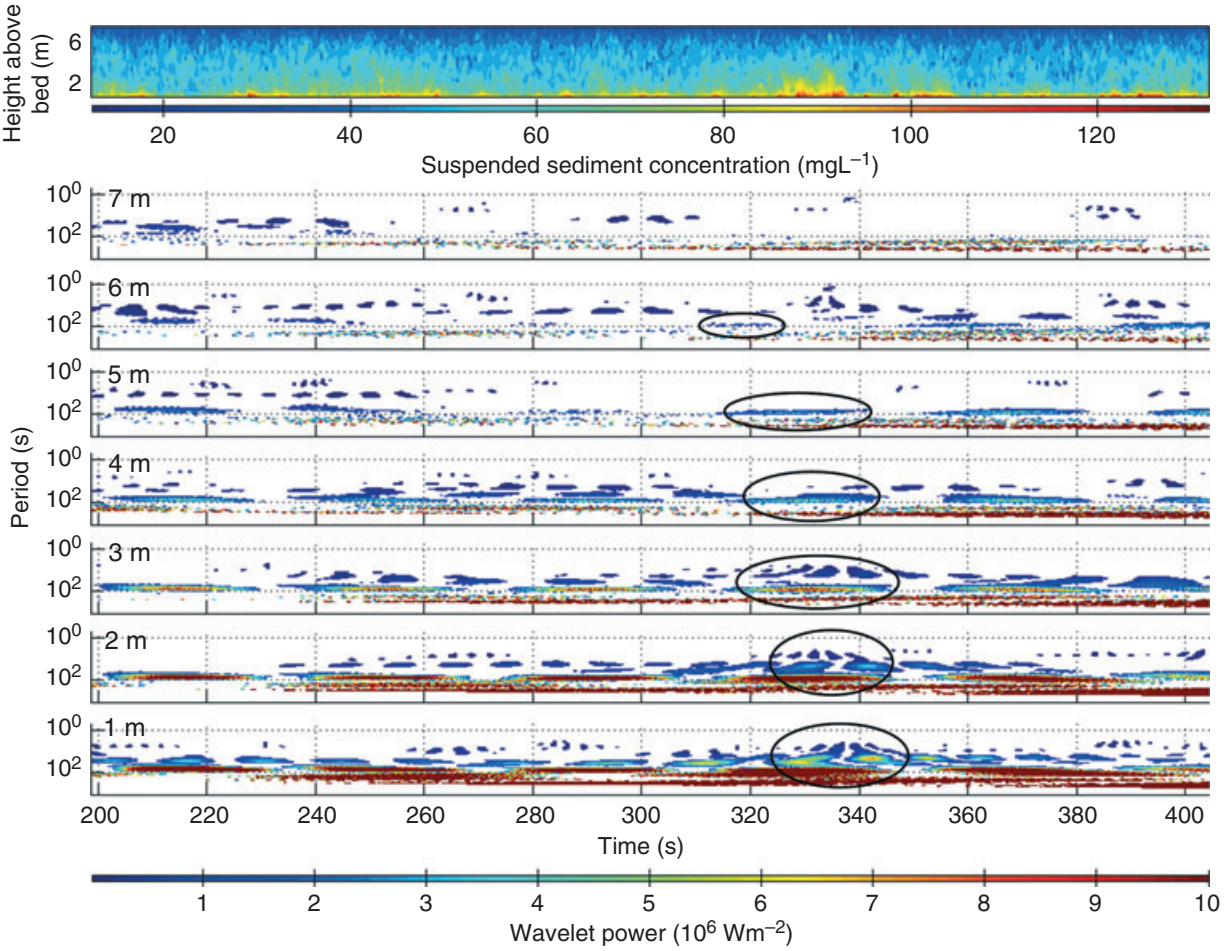

Fig. 9. Partial time series of calibrated suspended sediment concentration (SSC, top) collected over the dune crest and the corresponding vertical stack of local wavelet power spectra of calibrated SSC. Wavelet plots are labelled by height above the bed. Circles highlight evolution of a wavelet packet through the water column.

between 1 and 2 m above the bed). Longer-period structures generated near the bed persist higher into the flow than shorter period structures, which are often superimposed on the larger, more powerful lower-period structures. These high-frequency structures dissipate more rapidly with height above the bed than the lower frequency structures with which they are associated. A typical wavelet 'packet', or coherent flow structure, is traced through its evolution in the water column and circled on Fig. 9. Figure 10 shows the same evolving wavelet packet in greater detail.

At 1 m above the bed, between 300 and 350 sec in the time series, the circled packet (Fig. 10) appears to be composed of energy at two periodicities. The medium to low frequency, more powerful, packet has a period of 40 to 200 sec, with the wavelet power in the centre of the packet being $>10 \times 10^6$ W m^{-2}, whereas the higher frequency 'fingers' have a period of 5 to 40 sec and a peak wavelet power of 6×10^6 W m^{-2}. Higher in the flow, at 2 m above the bed, these structures split into three groups, again based primarily on period. The medium to low frequency packet retains a similar periodicity (45 to 150 sec with power $>10 \times 10^6$ W m^{-2}), whereas the higher frequency packet has split into two distinct groups with periods *ca* 10 to 40 sec and 5 to 10 sec, with associated peak wavelet power of $3{\cdot}5 \times 10^6$ and 1×10^6 W m^{-2}, respectively. At 3 m above the bed, the periodicity of the medium-frequency structures begins to become more focused, between 50 to 110 sec, with a slightly decreased peak wavelet power of 9×10^6 W m^{-2}. At this height, the medium-frequency structures appear to have separated from the higher frequency packets, leaving a group with period 5 to 10 sec and a wavelet power of 1×10^6 W m^{-2}. Above 3 m, the structures lose power sharply,

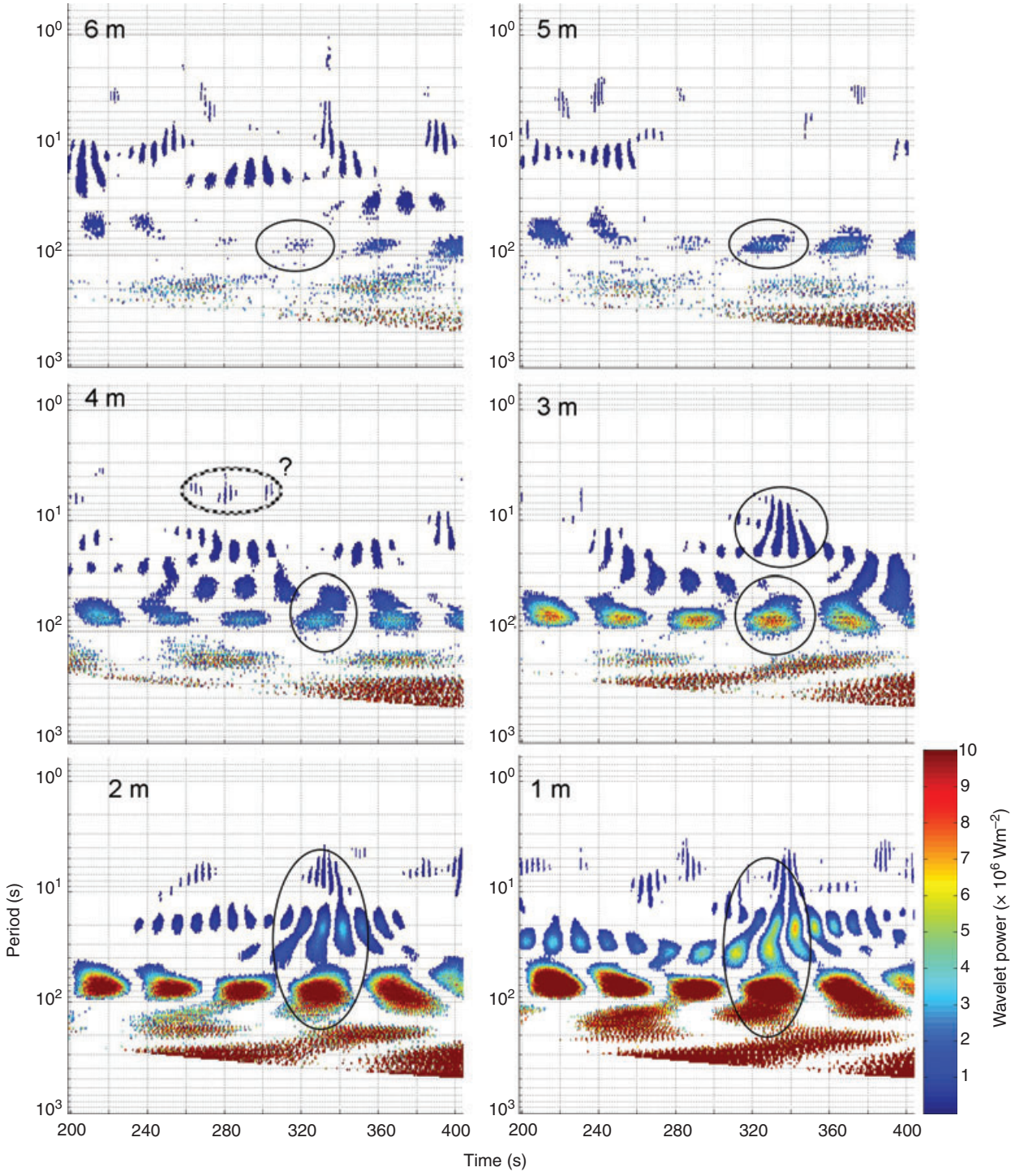

Fig. 10. More detail of the partial time series shown in Fig. 9, of the lower 6 m of a vertical stack of local wavelet power spectra of calibrated suspended sediment concentration. Wavelet plots are labelled by height above the bed. Circles highlight evolution of a wavelet packet through the water column.

peaking at only 4×10^6 W m^{-2} at 4 m above the bed. The medium-frequency packet at 4 m above the bed has a periodicity of 40 to 100 sec. It is difficult to pinpoint the location of the higher frequency packet, but it has probably advected downstream with a periodicity of only 4·5 to 7 sec and power of 1×10^6 W m^{-2}. This rapid decay in power appears to occur between 3 and 4 m above

the bed, or *ca* 0·45 of the flow depth of *ca* 7·5 m. At 5 m above the bed, the medium-frequency packet has a periodicity of 55 to 95 sec and a peak power of *ca* 3×10^6 W m^{-2}, whereas the higher frequency packets have all but disappeared. The medium-frequency packet is barely visible 6 m above the bed (observed between *ca* 310 and 330 sec in the series), with a period of 70 to 95 sec and a wavelet power of 1×10^6 W m^{-2} and disappears completely 7 m above the bed (Fig. 9). As these large-scale coherent flow structures interact with the flow surface, they generate 'boils' and a characteristic pattern of interaction that reflects the topology of the coherent flow structures (Best, 2005a). The pattern of energy and frequency dissipation observed here suggests that, nearer the bed, where velocity gradients are higher, large, long-period structures are generated in association with higher frequency and much less powerful structures. These higher-frequency structures lose coherence much more rapidly than the low-frequency packets as they rise towards the surface.

In a series of numerical and laboratory investigations of flow over dunes, Shimizu *et al.* (1999) and Schmeeckle *et al.* (1999) found a very similar pattern of turbulence evolution to the present study. At the shear layer downstream of a dune crest, Shimizu *et al.* (1999) found vigorous extraction of energy from the mean flow to transverse vortical structures. Just downstream of reattachment, these structures grew and became highly three-dimensional. Once the structures advected past the midpoint of the stoss side of the downstream dune, they began to break up into smaller vortical motions, with only the strongest of these vortices continuing to grow past the stoss midpoint and eventually erupting on the free surface (Best, 2005a). Shimizu *et al.* (1999) and Schmeeckle *et al.* (1999) explained the location of vortex breakup at the stoss midpoint as being due to the coherent flow structures reaching the peak of topographically induced flow acceleration. Itakura & Kishi (1980) similarly observed that small eddies generated at the upstream end of separation zones grew as they advected downstream. The resultant 'blob' of intensely turbulent fluid lifted from the reattachment point and eventually erupted as a boil on the free surface.

The patterns of flow and sediment transport observed over the study dune in the Río Paraná are consistent with other field, flume and numerical investigations. Streamwise velocity over the dune crest is inversely correlated with vertical velocity, with streamwise flow decelerations occurring simultaneously with vertical fluxes of fluid towards the water surface in the form of large fluid ejections. Regions of high SSC correlate well with such events. As discussed above, wavelet analysis of these turbulent events suggests that vortex shedding and wake flapping in the lee-side separation zone are the principal contributors to turbulence generation associated with such large alluvial sand dunes. Furthermore, turbulent flow structures, and their associated high SSCs, are seen to grow with height above the bed until a threshold height *ca* 0·45 of flow depth, above which they tend to decay and dissipate rapidly.

The association between vertical velocity and SSC identified in this study (for example, Fig. 7) echoes the findings of Schmeeckle *et al.* (1999) who demonstrated that the upward velocities present in vortical structures maintain the suspension of sediment. Nelson *et al.* (1993) argued that the acceleration of flow forced by the upsloping dune surface dampens the larger eddies by acceleration-induced vortex stretching, whereas McLean (2004) points out that the steepness of the topography downstream of the flow separation zone has a dramatic effect on the degree of flow acceleration. As acceleration of flow over the dune stoss is accompanied by a reduction in the strength and coherence of the coherent flow structure, the sediment rapidly falls out of suspension as the structures advect downstream and away from the bed. In the present study, the reduction in wavelet power and the number of wavelet packets with height (Figs 9 and 10) lends support to the interpretations of Shimizu *et al.* (1999) and Schmeeckle *et al.* (1999). Kadota & Nezu (1999) also discuss what they term 'separated vortices', in which parcels of fluid moving in the streamwise direction divide into two. One vortex moves towards the bed around the reattachment point, and the second vortex advances parallel to the flow direction. Additionally, some flow structures appear spontaneously above the bed and may represent events generated upstream that have risen towards the surface and propagated past the sensor, or they may be fragments that have separated from larger flow structures (e.g. Kostaschuk & Villard, 1996a). Further work to document fully the topology of turbulent flow structures generated over bedforms is required to elucidate the complex feedbacks between these structures, sediment transport and both dune morphology and migration.

CONCLUSIONS

The Río Paraná sand dune studied herein is asymmetric in downstream profile with a distinct 'brinkpoint' and lee-side slope. The temporally-averaged and spatially-averaged characteristics of flow documented herein are consistent with earlier field-based and flume-based research, including an increase in mean velocity and decrease in turbulence intensity with height above the bed, as well as a decrease in sand concentration with height above the bed.

Phase coherence wavelet analysis shows that streamwise and vertical velocities are strongly and inversely correlated over the dune crest, where flow decelerations are linked to fluid upwellings and vice versa. The inverse correlation between streamwise velocity and suspended sediment concentration (SSC), and the positive correlation between vertical velocity and SSC, indicate that fluid ejections sourced near the bed, and associated with lee-side flow separation, are suspending sand into the overlying flow.

Stacked series of wavelet plots indicate that clusters of low-frequency coherent flow structures initiate close to the bed, grow with height above the bed and then break up as they are advected downstream, with their decay possibly being linked to topographically-induced flow acceleration. The frequency at which these structures are generated is suitably predicted by the models of Driver *et al.* (1987) and Simpson (1989) for variation in separation zone size and wake flapping, respectively. However, the variability in the complex three-dimensional morphology of natural dunes may complicate these frequency relationships when compared to data obtained over simple two-dimensional steps derived from laboratory experiments.

The results of this study provide an example of the great value of wavelet analyses as compared to conventional spectral analysis based on Fourier transforms. All velocity and SSC time series display strongly intermittent coherent flow structures, especially near the bed. Hudgins *et al.* (1993) suggest that, to resolve such structures with Fourier techniques, it is necessary to know their size *a priori* and set the length of the window accordingly. However, as these flow structures differ in length throughout the time series, this cannot be accomplished simultaneously for all of these turbulent events. This study clearly demonstrates that wavelet analysis is a powerful tool for investigating such processes and illustrates its great potential in future research to elucidate a fuller understanding of the interactions between flow and sediment transport over complex topography.

ACKNOWLEDGEMENTS

JB, SL and DP would like to thank the UK Natural Environment Research Council (NERC) for award of Grants NER/A/S/2001/00445 and NER/B/S/2003/00243 that enabled this research to be undertaken. DP also thanks NERC for his Fellowship funding (NE/C002636/1). RK and DS thank the Natural Sciences and Engineering Research Council of Canada (grant RG1906-04) for additional support. The authors gratefully acknowledge the outstanding and full support of RESON (http://www.reson.com) in the field surveys. Additional thanks are due to the staff of CECOAL-CONICET (Corrientes, Argentina), in particular Casimiro Roberto, Luis Benetti and Roque Negro, as well as to Pam Montgomery for their field support. The authors would like to thank Mark Schmeeckle and one anonymous reviewer for their thoughtful and helpful insights and, in particular, Steve McLean for his detailed, thoughtful, incisive and constructive review that considerably assisted the analysis and final presentation.

NOTATION

A	constant, 0·22/°
α	lower brink angle
*	complex conjugate
B	constant, 6·473
C_D	drag coefficient
C	volume concentration of sand
$C_n^x(s)$	continuous wavelet transform
d	particle size
Δ	lower brink height
δ	flow depth
δt	time step
Fr	Froude number
f_s	dune-related turbulence frequency
f_s	Strouhal frequency
f_v	vortex shedding frequency
f_w	wake-flapping frequency
h	dune height
$\Im$	imaginary part of a wavelet transform
K_s	eddy diffusivity of sediment
N	number of data points
n	localized time index

η	dimensionless time
ϕ	phase
$\Psi(\eta)$	wavelet function
Re	Reynolds number
$\Re$	real part of a wavelet transform
ρ	water density
s	wavelet scale
τ_o	boundary shear stress
τ_{of}	form stress
τ_{os}	skin stress
τ_{ot}	sediment transport stress
$\bar{u}$	spatially-averaged velocity over the dune
u_*	shear velocity
U_o	spatially-averaged velocity upstream of step
U_s	temporally-averaged free stream velocity
w_s	grain settling velocity
W_n^{XY}	local wavelet cross-spectrum of X and Y
ω_o	dimensionless frequency
x_r	mean length of separation zone
x_n	time series
z	height above bed

REFERENCES

Adrian, R.J., Meinhart, C.D. and **Tomkins, C.D.** (2000) Vortex organization in the outer region of the turbulent boundary layer. *J. Fluid Mech.*, **422,** 1–54.

Agrawal, Y.C. and **Pottsmith, H.C.** (2000) Instruments for particle size and settling velocity observations in sediment transport. *Mar. Geol.*, **168,** 89–114.

Amsler, M.L. and **Garcia, M.H.** (1997) Sand-dune geometry of large rivers during floods: discussion. *J. Hydraul. Eng., ASCE*, **121,** 582–584.

Amsler, M.L., Prendes, H.H., Montagnini, M.D., Szupiany, R. and **Garcia, M.H.** (2003) Prediction of dune height in large sand-bed river: the case of the Paraná River, Argentina. In: *River, Coastal and Estuarine Morphodynamics* (Eds A. Sanchez-Arcilla and A. Bateman), IAHR Symposium, Barcelona, Spain, pp. 1104–1113.

Babakaiff, C.S. and **Hickin, E.J.** (1996) Coherent flow structures in Squamish River Estuary, British Columbia, Canada. In: *Coherent Flow Structures in Open Channels* (Eds P.J. Ashworth, S.J. Bennett, J.L. Best and S.J. McLelland), pp. 321–342. John Wiley and Sons Ltd, New York.

Bennett, S.J. and **Best, J.L.** (1995) Mean flow and turbulence structure over fixed, two-dimensional dunes: implications for sediment transport and bedform stability. *Sedimentology*, **42,** 491–513.

Best, J.L. (1993) On the interactions between turbulent flow structure, sediment transport and bedform development: some considerations from recent experimental research. In: *Turbulence: Perspectives on Flow and Sediment Transport* (Eds N.J. Clifford, J.R. French and J. Hardisty), pp. 61–92. John Wiley and Sons Ltd, New York.

Best, J.L. (1996) The fluid dynamics of small-scale alluvial bedforms. In: *Advances in Fluvial Dynamics and Stratigraphy* (Eds P.A. Carling and M.R. Dawson), pp. 67–125. John Wiley and Sons Ltd, Chichester, UK.

Best, J.L. (2005a) The kinematics, topology and significance of dune-related macroturbulence: some observations from the laboratory and field. In: *Fluvial Sedimentology VII* (Eds M.D. Blum, S.B. Marriott and S. LeClair), *Int. Assoc. Sedimentol. Spec. Publ.*, **35,** 41–60.

Best, J.L. (2005b) The fluid dynamics of river dunes: a review and some future research directions. *J. Geophys. Res., Earth Surf.*, **110,** F04S02; doi: 10.1029/2004JF000218.

Best, J.L. and **Kostaschuk, R.A.** (2002) An experimental study of turbulent flow over a low-angle dune. *J. Geophys. Res.*, **107,** 1–19.

Best, J.L., Kostaschuk, R.A. and **Villard, P.V.** (2001) Quantitative visualization of flow fields associated with alluvial sand dunes: results from the laboratory and field using ultrasonic and acoustic Doppler anemometry. *J. Vis.*, **4,** 373–381.

Bjerkås, M. (2006) Wavelet transforms and ice action on structures. *Cold Reg. Sci. Technol.*, **44,** 159–169.

Bonetto, A.A. and **Orfeo, A.** (1984) Caracteres sedimentologicos de la carga en suspension del Río Parana entre confluencia Y esquina (Prov. De Corrientes, R.A.). *Rev. As. Argentina de Min., Pet. y Sed.*, **15,** 51–61.

Carling, P.A., Williams, J.J., Gölz, E. and **Kelsey, A.D.** (2000) The morphodynamics of fluvial sand dunes in the River Rhine, near Mainz, Germany. II. Hydrodynamics and sediment transport. *Sedimentology*, **47,** 253–278.

Clifford, N.J. and **French, J.R.** (1993) Monitoring and modelling turbulent flow: historical and contemporary perspectives. In: *Turbulence: Perspectives on Flow and Sediment Transport* (Eds N.J. Clifford, J.R. French and J. Hardisty), pp. 1–34. John Wiley and Sons Ltd, New York.

Coleman, S.E., Nikora, V.I., McLean, S.R., Clunie, T.M., Schlicke, T. and **Melville, B.W.** (2006) Equilibrium hydrodynamics concept for developing dunes. *Phys. Fluids*, **18,** 105104; doi: 10.1063/1.2358332.

Driver, D.M., Seegmiller, H.L. and **Marvin, J.G.** (1987) Time-dependent behavior of a reattaching shear layer. *AIAA J.*, **25,** 914–919.

Engel, P. (1981) Length of flow separation over dunes. *J. Hydraul. Div., ASCE*, **107,** 1133–1143.

Farge, M. (1992) Wavelet transforms and their application to turbulence. *Annu. Rev. Fluid Mech.*, **24,** 395–457.

Fernandez, R., Best, J. and **López, F.** (2006) Mean flow, turbulence structure, and bed form superimposition across the ripple-dune transition. *Water Resour. Res.*, **42,** W05406; doi: 10.1029/2005WR004330.

Gomes, L.C. and **Miranda, L.E.** (2001) Hydrologic and climatic regimes limit phytoplankton biomass in reservoirs of the Upper Paraná River Basin, Brazil. *Hydrobiologia*, **457,** 205–214.

Grass, A.J. (1971) Structural features of turbulent flow over smooth and rough boundaries. *J. Fluid Mech.*, **50,** 233–255.

Hudgins, L., Friehe, C.A. and **Mayer, M.E.** (1993) Wavelet transforms and atmospheric turbulence. *Phys. Rev. Lett.*, **71,** 3279–3283.

Itakura, T. and **Kishi, T.** (1980) Open channel flow with suspended sediment on sand waves. In: *Proc of the Third Intl Symposium on Stochastic Hydraulics* (Eds H. Kikkawa and Y. Iwasa), *Int. Assoc. Hydraul. Res.*, pp. 599–609. Tokyo.

Jackson, R.G. (1976) Sedimentological and fluid-dynamic implications of the turbulent bursting phenomena in geophysical flows. *J. Fluid Mech.*, **50,** 133–160.

Johns, B., Soulsby, R.L. and **Chesher, T.J.** (1990) The modelling of sandwave evolution resulting from suspended and bed-load transport of sediment. *J. Hydraul. Res.*, **28,** 355–374.

Johns, B., Soulsby, R.L. and **Xing, J.** (1993) A comparison of numerical model experiments of free surface flow over topography with flume and field experiments. *J. Hydraul. Res.*, **31,** 215–228.

Kadota, A. and **Nezu, I.** (1999) Three-dimensional structure of space-time correlation on coherent vortices generated behind dune crest. *J. Hydraul. Res.*, **37,** 59–80.

Kline, S.J., Reynolds, W.C., Schraub, F.A. and **Runstadler, P.W.** (1967) The structure of turbulent boundary layers. *J. Fluid Mech.*, **30,** 741–773.

Kostaschuk, R.A. (2000) A field study of turbulence and sediment dynamics over subaqueous dunes with flow separation. *Sedimentology*, **47,** 519–531.

Kostaschuk, R.A. and **Church, M.A.** (1993) Macroturbulence generated by dunes: Fraser River, Canada. *Sed. Geol.*, **85,** 25–37.

Kostaschuk, R.A. and **Ilersich, S.A.** (1995) Dune geometry and sediment transport: Fraser River, British Columbia. In: *River Geomorphology* (Ed E. Hickin), pp. 19–36. John Wiley & Sons Ltd, New York.

Kostaschuk, R.A. and **Villard, P.** (1996a) Turbulent sand suspension events: Fraser River, Canada. In: *Coherent Flow Structures in Open Channels* (Eds P.J. Ashworth, S.J. Bennett, J.L. Best and S.J. McLelland), pp. 305–318. John Wiley and Sons Ltd, New York.

Kostaschuk, R.A. and **Villard, P.** (1996b) Flow and sediment transport over large subaqueous dunes: Fraser River, Canada. *Sedimentology*, **4,** 849–863.

Kostaschuk, R.A. and **Villard, P.** (1999) Turbulent sand suspension over dunes. In: *Fluvial Sedimentology VI* (Eds N.D. Smith and J. Rogers), *Int. Assoc. Sedimentol. Spec. Publ.*, **28,** 3–13.

Kostaschuk, R.A., Terry, J. and **Raj, R.** (2003) Suspended sediment transport during tropical-cyclone floods in Fiji. *Hydrol. Process.*, **17,** 1149–1164.

Kostaschuk, R.A., Villard, P. and **Best, J.** (2004) Measuring velocity and shear stress over dunes with acoustic Doppler profiler. *J. Hydraul. Eng., ASCE*, **130,** 932–936.

Kostaschuk, R.A., Best, J., Villard, P., Peakall, J. and **Franklin, M.** (2005) Measuring velocity and sediment transport with an acoustic Doppler profiler. *Geomorphology*, **68,** 25–38.

Lafrenière, M. and **Sharp, M.** (2003) Wavelet analysis of inter-annual variability in the runoff regimes of glacial and nival stream catchments, Bow Lake, Alberta. *Hydrol. Process.*, **17,** 1093–1118.

Lane, S.N. (2007) Assessment of rainfall-runoff models based upon wavelet analysis. *Hydrol. Process.*, **21,** 586–607.

Lapointe, M. (1992) Burst-like sediment suspension events in a sand bed river. *Earth Surf. Proc. Land.*, **17,** 253–270.

Levi, E. (1983) A universal Strouhal law. *J. Eng. Mech.*, **109,** 718–727.

Levi, E. (1991) Vortices in hydraulics. *J. Hydraul. Eng.*, **117,** 399–413.

Liandrat, J. and **Moret-Bailly, F.** (1990) The wavelet transform: some applications to fluid dynamics and turbulence. *Eur. J. Mech., B/Fluids*, **9,** 1–19.

Maddux, T.B., McLean, S.R. and **Nelson, J.M.** (2003) Turbulence flow over three-dimensional dunes: 2. Fluid and bed stresses. *J. Geophys. Res.*, **108,** F1; doi: 10.1029/2003JF000018.

Maraun, D. and **Kurths, J.** (2004) Cross wavelet analysis: significance testing and pitfalls. *Nonlinear Process. Geophys.*, **11,** 505–514.

Matthes, G.H. (1947) Macroturbulence in natural stream flow. *Trans. Am. Geophys. Union*, **28,** 255–262.

McLean, S. (2004) The effect of bedform-induced spatial acceleration on turbulence and sediment transport. In: *Marine Sandwave and River Dune Dynamics II* (Eds S. Hulscher, T. Garlan and D. Idier), pp. 216–223. University of Twente, The Netherlands.

McLean, S.R. and **Smith, J.D.** (1979) Turbulence measurements in the boundary layer over a sand wave field. *J. Geophys. Res.*, **84,** 7,791–7808.

McLean, S.R., Nelson, J.M. and **Wolfe, S.R.** (1994) Turbulence structure over two-dimensional bed forms: implications for sediment transport. *J. Geophys. Res.*, **99,** 12,729–12747.

Müller, A. and **Gyr, A.** (1986) On the vortex formation in the mixing layer behind dunes. *J. Hydraul. Res.*, **24,** 359–375.

Nelson, J.M. and **Smith, J.D.** (1989) Mechanics of flow over ripples and dunes. *J. Geophys. Res. Oceans*, **94,** 8146–8162.

Nelson, J.M., McLean, S.R. and **Wolfe, S.R.** (1993) Mean flow and turbulence fields over two-dimensional bedforms. *Water Resour. Res.*, **29,** 3935–3953.

Nezu, I. and **Nakagawa, H.** (1993) *Turbulence in Open-Channel Flows*. IAHR Monograph, Balkema, Rotterdam, 281 pp.

Orfeo, O. and **Stevaux, J.** (2002) Hydraulic and morphological characteristics of middle and upper reaches of the Paraná River (Argentina and Brazil). *Geomorphology*, **44,** 309–322.

Parsons, D.R., Best, J.L., Orfeo, O., Hardy, R.J., Kostaschuk, R. and **Lane, S.N.** (2005) The morphology and flow fields of three-dimensional dunes, Río Paraná, Argentina: results from simultaneous multibeam echo sounding and acoustic Doppler current profiling. *J. Geophys. Res.*, **110,** F04S03; doi: 10.1029/2004JF000231.

van Rijn, L.C. (1984) Sediment transport, part III: bed forms and alluvial roughness. *J. Hydraulic Eng.*, **110,** 1733–1754.

van Rijn, L.C. (1993) *Principles of Sediment Transport in Rivers, Estuaries and Coastal Seas*. Aqua Publications, Amsterdam, The Netherlands, 700 pp.

Robinson, S.K. (1991) Coherent motions in the turbulent boundary layer. *Ann. Rev. Fluid. Mech.*, **23,** 601–639.

Roy, A.G., Buffin-Bélanger, T., Lamarre, H. and **Kirkbride, A.D.** (2004) Size, shape and dynamics of large-scale turbulent flow structures in a gravel-bed river. *J. Fluid Mech.*, **500,** 1–27.

Schatz, V. and **Herrmann, H.J.** (2006) Flow separation in the lee of transverse dunes: a numerical investigation. *Geomorphology*, **81,** 207–216.

Schmeeckle, M.W., Shimizu, Y., Hoshi, K., Baba, H. and **Ikezaki, S.** (1999) Turbulent structures and suspended sediment over two-dimensional dunes. In: *River, Coastal and Estuarine Morphodynamics* (Ed. G. Seminara), IAHR Symposium, Genova, Italy, pp. 261–270.

Shimizu, Y., Schmeeckle, M.W., Hoshi, K. and **Tateya, K.** (1999) Numerical simulation of turbulence over two-dimensional dunes. In: *River, Coastal and Estuarine Morphodynamics* (Ed. G. Seminara), IAHR Symposium, Genova, Italy, pp. 251–260.

Shugar, D.H. (2005) *The Dynamics and Evolution of Coherent Flow Structures Over Dunes, Parana River, Argentina*. Unpubl. MSc thesis, University of Guelph, 151 pp.

Simpson, R.L. (1989) Turbulent boundary-layer separation. *Annu. Rev. Fluid Mech.*, **21,** 205–234.

Smith, C.R. (1996) Coherent Flow Structures in Flat Wall Turbulent Boundary Layers: facts, Mechanisms, and Speculation. In: *Coherent Flow Structures in Open Channels* (Eds P.J. Ashworth, S.J. Bennett, J.L. Best and S.J. McLelland), pp. 1–39. John Wiley and Sons Ltd, New York.

Smith, J.D. and **McLean, S.R.** (1977) Spatially averaged flow over a wavy surface. *J. Geophys. Res.*, **82,** 1735–1746.

Soulsby, R.L. (1997) *Dynamics of Marine Sands: A Manual for Practical Applications*. Thomas Telford, London, 249 pp.

Stoesser, T., Braun, C., Garcia-Villalba, M. and **Rodi, W.** (2008) Turbulence structures in flow over two dimensional dunes, *J. Hydraul. Eng.*, **134,** 42–55.

Tennekes, H. and **Lumley, J.L.** (1972) *A First Course in Turbulence*. MIT Press, Cambridge, Mass., 300 pp.

Torrence, C. and **Compo, G.P.** (1998) A practical guide to wavelet analysis. *Bull. Am. Met. Soc.*, **79,** 62–78.

Torrence, C. and **Webster, P.J.** (1999) Interdecadal changes in the ENSO-monsoon system. *J. Clim.*, **12,** 2679–2690.

Venditti, J.G. (2003) *Initiation and Development of Sand Dunes in River Channels*. Unpubl. PhD thesis, UBC, 315 pp.

Venditti, J.G. and **Bauer, B.O.** (2005) Turbulent flow over a dune: Green River, Colorado. *Earth Surf. Proc. Land.*, **30,** 289–304.

Venditti, J.G. and **Bennett, S.J.** (2000) Spectral analysis of turbulent flow and suspended sediment transport over fixed dunes, *J. Geophys. Res.*, **105,** 22035–22047.

Villard, P.V. and **Kostaschuk, R.A.** (1998) The relation between shear velocity and suspended sediment concentration over dunes: Fraser Estuary, Canada. *Mar. Geol.*, **148,** 71–81.

Wilbers, A. (2004) *The Development and Hydraulic Roughness of Subaqueous Dunes*. PhD Thesis, Faculty of Geosciences, Utrecht University, Netherlands Geographical Studies 323, 227 pp.

Williams, J.J., Bell, P.S. and **Thorne, P.D.** (2003) Field measurements of flow fields and sediment transport above mobile bed forms. *J. Geophys. Res.*, **108**(C4), 6.1–6.36. Art. No. 3109.

Yalin, M.S. (1992) *River Mechanics*. Pergamon Press, Oxford, 219 pp.

Yue, W., Lin, C.L. and **Patel, V.C.** (2005) Large eddy simulation of turbulent open-channel flow with free surface simulated by level set method. *Phys. Fluids*, **17,** 025108–025112; doi: 1070-6631/2005/17(2)/025108/12.

Zalocar de Domitrovic, Y. (2005) Biodiversidad del fitoplancton en el eje fluvial Paraguay-Paraná. In: *Temas de la Biodiversidad del litoral fluvial Argentino, INSUGEO* (Ed. F.G. Aceñolaza), *Miscelánea*, **14,** 229–242.

Manuscript received 6 September 2007; revision accepted 2 September 2009